



Two Ultra-faint Milky Way Stellar Systems Discovered in Early Data from the DECam Local Volume Exploration Survey

S. Mau^{1,2} , W. Cerny^{1,2} , A. B. Pace³ , Y. Choi⁴ , A. Drlica-Wagner^{1,2,5} , L. Santana-Silva⁶ , A. H. Riley⁷ , D. Erkal⁸ , G. S. Stringfellow⁹ , M. Adamów¹⁰ , J. L. Carlin¹¹ , R. A. Gruendl^{10,12} , D. Hernandez-Lang^{13,14,15}, N. Kuropatkin⁵ , T. S. Li^{16,17,45} , C. E. Martínez-Vázquez¹⁴ , E. Morganson¹⁰ , B. Mutlu-Pakdil¹⁸ , E. H. Neilsen⁵ , D. L. Nidever^{19,20} , K. A. G. Olsen²⁰ , D. J. Sand¹⁸ , E. J. Tollerud⁴ , D. L. Tucker⁵ , B. Yanny⁵ , A. Zenteno¹⁴, S. Allam⁵ , W. A. Barkhouse²¹ , K. Bechtol²² , E. F. Bell²³ , P. Balaji^{1,2} , D. Crnojević^{24,25} , J. Esteves²⁶, P. S. Ferguson⁷ , C. Gallart^{27,28} , A. K. Hughes¹⁸ , D. J. James^{29,30} , P. Jethwa³¹ , L. C. Johnson³² , K. Kuehn^{33,34} , S. Majewski³⁵ , Y.-Y. Mao^{36,45} , P. Massana⁸ , M. McNanna²² , A. Monachesi^{37,38} , E. O. Nadler^{39,40} , N. E. D. Noël⁸ , A. Palmese⁵ , F. Paz-Chinchon¹⁰ , A. Pieres^{41,42} , J. Sanchez⁵ , N. Shipp^{1,2,5} , J. D. Simon¹⁶, M. Soares-Santos^{5,26} , K. Tavangar^{1,2} , R. P. van der Marel^{4,43} , A. K. Vivas¹⁴ , A. R. Walker¹⁴ , and R. H. Wechsler^{39,40,44}

(DELVE Collaboration)

¹ Kavli Institute for Cosmological Physics, University of Chicago, Chicago, IL 60637, USA; sidneymau@uchicago.edu, williamcerny@uchicago.edu, kadrlica@fnal.gov

² Department of Astronomy and Astrophysics, University of Chicago, Chicago IL 60637, USA

³ McWilliams Center for Cosmology, Carnegie Mellon University, 5000 Forbes Avenue, Pittsburgh, PA 15213, USA

⁴ Space Telescope Science Institute, 3700 San Martin Drive, Baltimore, MD 21218, USA

⁵ Fermi National Accelerator Laboratory, P.O. Box 500, Batavia, IL 60510, USA

⁶ Federal University of Rio de Janeiro, Valongo Observatory, Ladeira Pedro Antonio, 43, Saúde 20080-090 Rio de Janeiro, Brazil

⁷ George P. and Cynthia Woods Mitchell Institute for Fundamental Physics and Astronomy, and Department of Physics and Astronomy, Texas A&M University, College Station, TX 77843, USA

⁸ Department of Physics, University of Surrey, Guildford GU2 7XH, UK

⁹ Center for Astrophysics and Space Astronomy, University of Colorado, 389 UCB, Boulder, CO 80309-0389, USA

¹⁰ National Center for Supercomputing Applications, University of Illinois, 1205 West Clark Street, Urbana, IL 61801, USA

¹¹ LSST, 950 North Cherry Avenue, Tucson, AZ, 85719, USA

¹² Department of Astronomy, University of Illinois, 1002 W. Green Street, Urbana, IL 61801, USA

¹³ University of La Serena, La Serena, Chile

¹⁴ Cerro Tololo Inter-American Observatory, NSF's National Optical-Infrared Astronomy Research Laboratory, Casilla 603, La Serena, Chile

¹⁵ Gemini Observatory, La Serena, Chile

¹⁶ Observatories of the Carnegie Institution for Science, 813 Santa Barbara Street, Pasadena, CA 91101, USA

¹⁷ Department of Astrophysical Sciences, Princeton University, Princeton, NJ 08544, USA

¹⁸ Department of Astronomy/Steward Observatory, 933 North Cherry Avenue, Room N204, Tucson, AZ 85721-0065, USA

¹⁹ Department of Physics, Montana State University, P.O. Box 173840, Bozeman, MT 59717-3840, USA

²⁰ NSF's National Optical-Infrared Astronomy Research Laboratory, 950 N. Cherry Ave., Tucson, AZ 85719, USA

²¹ Department of Physics and Astrophysics, University of North Dakota, Grand Forks, ND 58202, USA

²² Department of Physics, University of Wisconsin-Madison, Madison, WI 53706, USA

²³ Department of Astronomy, University of Michigan, 1085 S. University Avenue, Ann Arbor, MI 48109, USA

²⁴ Department of Chemistry and Physics, University of Tampa, 401 West Kennedy Boulevard, Tampa, FL 33606, USA

²⁵ Department of Physics & Astronomy, Texas Tech University, Box 41051, Lubbock, TX 79409, USA

²⁶ Department of Physics, Brandeis University, Waltham, MA 02453, USA

²⁷ Instituto de Astrofísica de Canarias, La Laguna, Tenerife, Spain

²⁸ Departamento de Astrofísica, Universidad de La Laguna, Tenerife, Spain

²⁹ Center for Astrophysics, Harvard & Smithsonian, 60 Garden Street, Cambridge, MA 02138, USA

³⁰ Black Hole Initiative at Harvard University, 20 Garden Street, Cambridge, MA 02138, USA

³¹ Institute for Astrophysics, Türkenschanzstraße 17, A-1180 Wien, Austria

³² Center for Interdisciplinary Exploration and Research in Astrophysics (CIERA) and Department of Physics and Astronomy, Northwestern University, 2145 Sheridan Road, Evanston, IL 60208, USA

³³ Lowell Observatory, 1400 W Mars Hill Road, Flagstaff, AZ 86001, USA

³⁴ Australian Astronomical Optics, Macquarie University, North Ryde, NSW 2113, Australia

³⁵ Department of Astronomy, University of Virginia, Charlottesville, VA, 22904, USA

³⁶ Department of Physics and Astronomy, Rutgers, The State University of New Jersey, Piscataway, NJ 08854, USA

³⁷ Instituto de Investigación Multidisciplinar en Ciencia y Tecnología, Universidad de La Serena, Raúl Bitrán 1305, La Serena, Chile

³⁸ Departamento de Astronomía, Universidad de La Serena, Av. Juan Cisternas 1200 Norte, La Serena, Chile

³⁹ Department of Physics, Stanford University, 382 Via Pueblo Mall, Stanford, CA 94305, USA

⁴⁰ Kavli Institute for Particle Astrophysics & Cosmology, P.O. Box 2450, Stanford University, Stanford, CA 94305, USA

⁴¹ Instituto de Física, UFRGS, Caixa Postal 15051, Porto Alegre, RS—91501-970, Brazil

⁴² Laboratório Interinstitucional de e-Astronomia—LIneA, Rua Gal. José Cristino 77, Rio de Janeiro, RJ—20921-400, Brazil

⁴³ Center for Astrophysical Sciences, Department of Physics & Astronomy, Johns Hopkins University, Baltimore, MD 21218, USA

⁴⁴ SLAC National Accelerator Laboratory, Menlo Park, CA 94025, USA

Received 2019 December 5; accepted 2020 January 14; published 2020 February 21

⁴⁵ NHFP Einstein Fellow.

Abstract

We report the discovery of two ultra-faint stellar systems found in early data from the DECam Local Volume Exploration survey (DELVE). The first system, Centaurus I (DELVE J1238–4054), is identified as a resolved overdensity of old and metal-poor stars with a heliocentric distance of $D_{\odot} = 116.3^{+0.6}_{-0.6}$ kpc, a half-light radius of $r_h = 2.3^{+0.4}_{-0.3}$ arcmin, an age of $\tau > 12.85$ Gyr, a metallicity of $Z = 0.0002^{+0.0001}_{-0.0002}$, and an absolute magnitude of $M_V = -5.55^{+0.11}_{-0.11}$ mag. This characterization is consistent with the population of ultra-faint satellites and confirmation of this system would make Centaurus I one of the brightest recently discovered ultra-faint dwarf galaxies. Centaurus I is detected in *Gaia* DR2 with a clear and distinct proper motion signal, confirming that it is a real association of stars distinct from the Milky Way foreground; this is further supported by the clustering of blue horizontal branch stars near the centroid of the system. The second system, DELVE 1 (DELVE J1630–0058), is identified as a resolved overdensity of stars with a heliocentric distance of $D_{\odot} = 19.0^{+0.5}_{-0.6}$ kpc, a half-light radius of $r_h = 0.97^{+0.24}_{-0.17}$ arcmin, an age of $\tau = 12.5^{+1.0}_{-0.7}$ Gyr, a metallicity of $Z = 0.0005^{+0.0002}_{-0.0001}$, and an absolute magnitude of $M_V = -0.2^{+0.8}_{-0.6}$ mag, consistent with the known population of faint halo star clusters. Given the low number of probable member stars at magnitudes accessible with *Gaia* DR2, a proper motion signal for DELVE 1 is only marginally detected. We compare the spatial position and proper motion of both Centaurus I and DELVE 1 with simulations of the accreted satellite population of the Large Magellanic Cloud (LMC) and find that neither is likely to be associated with the LMC.

Unified Astronomy Thesaurus concepts: Dwarf galaxies (416); Local Group (929); Star clusters (1567); Milky Way Galaxy (1054)

1. Introduction

Ultra-faint dwarf galaxies are the least luminous and most dark-matter-dominated objects in the known universe. They are generally characterized by their low luminosities, relatively large mass-to-light ratios, and old, metal-poor stellar populations (e.g., McConnachie 2012; Drlica-Wagner et al. 2019a; Simon 2019, and references therein). As dark-matter-dominated systems, ultra-faint galaxies are among the most pristine laboratories for the study of dark matter itself. For instance, they serve as excellent candidates for the indirect detection of dark matter annihilation and decay (e.g., Geringer-Sameth et al. 2015; Albert et al. 2017). Furthermore, the census of Milky Way satellite galaxies has been used to constrain models of particle dark matter (e.g., cold, warm, and self-interacting dark matter), which predict different structures at small scales (e.g., Aaronson 1983; Macciò & Fontanot 2010; Lovell et al. 2014; Jethwa et al. 2018; Nadler et al. 2019a). The demographics of the Milky Way satellite population have been used to test our understanding of reionization (e.g., Boylan-Kolchin et al. 2015), the formation of the smallest galaxies (e.g., Jeon et al. 2017; Wheeler et al. 2019), the galaxy–halo connection (e.g., Jethwa et al. 2018; Kim et al. 2018; Newton et al. 2018; Nadler et al. 2019b), and the origin of the heavy elements (e.g., Ji et al. 2016; Frebel 2018). As such, there has been great interest in the discovery, confirmation, and characterization of new faint systems.

Faint halo star clusters form another population of stellar systems in orbit around the Milky Way. While their surface brightnesses are comparable to those of the ultra-faint galaxies, they are generally characterized by having smaller physical sizes ($r_{1/2} \lesssim 20$ pc) and heliocentric distances ($D_{\odot} \gtrsim 15$ kpc) than dark-matter-dominated satellite galaxies. These faint star clusters are proposed to have been accreted onto the Milky Way through the disruption of infalling satellite galaxies (e.g., Gnedin & Ostriker 1997; Searle & Zinn 1978; Koposov et al. 2007; Forbes & Bridges 2010; Leaman et al. 2013; Massari et al. 2017). As such, understanding the population of faint halo star clusters is an important aspect in understanding the assembly history of the Milky Way. While physical sizes can be used as a proxy to categorize objects as either ultra-faint

galaxies or faint star clusters, the most definitive classification comes from the kinematic measurement of dark matter content via spectroscopic analysis.

Before the advent of the Sloan Digital Sky Survey (SDSS), there were only a dozen known Milky Way satellite galaxies. The unprecedented depth of SDSS over most of the northern sky resulted in a doubling of the known population of satellite galaxies during the decade from 2005 to 2015 (e.g., Willman et al. 2005a, 2005b; Belokurov et al. 2006, 2007, 2009, 2010; Zucker et al. 2006a, 2006b). By virtue of successive large sky surveys, including those using the Dark Energy Camera (DECam; Flaugher et al. 2015) installed on the 4 m Blanco Telescope at the Cerro Tololo Inter-American Observatory in Chile, the current number of Milky Way satellite galaxies has increased to ~ 60 in the past five years. Simultaneously, new star clusters have been discovered at increasingly faint magnitudes, contributing to the overall population of stellar systems orbiting the Milky Way. Specifically, searches for Milky Way satellites in the Dark Energy Survey (DES; e.g., Bechtol et al. 2015; Drlica-Wagner et al. 2015; Kim & Jerjen 2015a; Koposov et al. 2015; Luque et al. 2016) and Pan-STARRS (e.g., Laevens et al. 2014, 2015a, 2015b) resulted in the discovery of more than 20 new satellites. Deep imaging surveys using the Hyper Suprime-Cam have also uncovered three new candidate dwarf galaxies at distances and brightnesses inaccessible to previous surveys (Homma et al. 2016, 2018, 2019). Meanwhile, there have been a number of community-led DECam surveys that have contributed to the census of Milky Way satellites. These include the Survey of the MAGellanic Stellar History (SMASH; e.g., Martin et al. 2015; Nidever et al. 2017), the Magellanic SatELites Survey (MagLiteS; e.g., Drlica-Wagner et al. 2016; Torrealba et al. 2018), the Magellanic Edges Survey (e.g., Koposov et al. 2018), and the Blanco Imaging of the Southern Sky Survey (e.g., Mau et al. 2019). With increasing sky coverage and depth, DECam is expected to continue to play an important role in searching for ultra-faint Milky Way satellites in the southern sky. We refer the reader to Simon (2019) and references therein for a recent review of the Milky Way ultra-faint satellite galaxy population.

As a continuation of these community-led surveys in the southern hemisphere, the DECam Local Volume Exploration survey (DELVE)⁴⁶ seeks to complete DECam coverage of the southern sky with $|b| > 10^\circ$ by combining 126 nights of new observations in the 2019A–2021B semesters with existing public DECam community data. DELVE consists of three survey components: a shallow wide-area survey of the southern sky (WIDE), a medium-depth survey around the Magellanic Clouds (MC; this serves as an extension of SMASH and MagLiteS), and a deep-drilling survey around four Magellanic analogs in the Local Volume (DEEP; e.g., similar to Sand et al. 2015 and Carlin et al. 2016). In particular, DELVE-WIDE is designed to search for new ultra-faint stellar systems around the Milky Way by mapping the high-Galactic-latitude southern sky to a depth comparable to that of the first two years of DES.

Using an early version of the DELVE-WIDE catalog, which was constructed from existing public DECam exposures and DELVE exposures that were taken primarily in 2019A, we conducted a search for new faint Milky Way satellites and found two new resolved stellar overdensities that are consistent with old, metal-poor isochrones. Furthermore, we cross-matched the early DELVE-WIDE data with the *Gaia* DR2 catalog (Gaia Collaboration et al. 2018) in the regions around these systems and measured their proper motions, helping confirm that these systems are real associations of stars. The first of these systems, DELVE J1238–4054, has a physical size and luminosity consistent with the locus of ultra-faint galaxies (Table 1, Figure 5), and we tentatively denote it Centaurus I (Cen I). In contrast, the small physical size and extremely low luminosity of the second system, DELVE J1630–0058, are consistent with the population of faint halo star clusters (Table 1, Figure 5), and we tentatively assign it the name DELVE 1. We note that this system was simultaneously discovered in Pan-STARRS DR1 (Drlica-Wagner et al. 2019a). While kinematic measurements are necessary to definitively classify the nature of faint stellar systems, this labeling scheme follows the convention of naming ultra-faint galaxies after the constellation in which they reside and faint star clusters after the survey in which they were discovered.

This paper is organized as follows. In Section 2, we describe DELVE-WIDE and the early catalog used in this study. The search algorithm is described in Section 3. In Section 4, we present the morphology, isochrone parameters, and proper motions of Centaurus I and DELVE 1. Finally, in Section 5, we discuss interesting features of each system as well as their possible origins. We briefly conclude in Section 6.

2. Data

DELVE-WIDE seeks to achieve complete, contiguous coverage of the high-Galactic-latitude ($|b| > 10^\circ$) southern sky in g, r, i, z by targeting regions of the sky that have not been observed by other community programs. DELVE is expected to collect ~20,000 new exposures over its three-year survey. During the first year of DELVE observing, we performed 3×90 s dithered exposures in g, i following the survey strategy of DES. We leave a detailed description of DELVE observing and data reduction to a future paper.

Our early DELVE-WIDE data set consists of approximately 14,000 exposures in the northern Galactic cap with $b > 10^\circ$ and $\delta_{2000} < 0^\circ$. The main constituents of this data set are

Table 1
Derived Morphology, Isochrone, and Proper Motion Parameters for Centaurus I and DELVE 1

Parameter	Centaurus I	DELVE 1
α_{2000} (deg)	$189.585^{+0.004}_{-0.004}$	$247.725^{+0.002}_{-0.002}$
δ_{2000} (deg)	$-40.902^{+0.004}_{-0.005}$	$-0.972^{+0.003}_{-0.003}$
a_h (arcmin)	$2.9^{+0.5}_{-0.4}$	$1.10^{+0.27}_{-0.19}$
r_h (arcmin)	$2.3^{+0.4}_{-0.3}$	$0.97^{+0.24}_{-0.17}$
$r_{1/2}$ (pc)	79^{+14}_{-10}	$5.4^{+1.5}_{-1.1}$
ϵ	$0.4^{+0.1}_{-0.1}$	$0.2^{+0.1}_{-0.2}$
P.A. (deg)	20^{+11}_{-11}	21^{+26}_{-30}
$m - M$ (mag)	$20.33^{+0.03}_{-0.01} \pm 0.1^a$	$16.39^{+0.06}_{-0.07} \pm 0.1^a$
D_\odot (kpc)	$116.3^{+1.6}_{-0.6}$	$19.0^{+0.5}_{-0.6}$
τ (Gyr)	$> 12.85^b$	$12.5^{+1.0}_{-0.7}$
Z	$0.0002^{+0.0001}_{-0.0002}$	$0.0005^{+0.0002}_{-0.0001}$
$\sum_i P_{i,\text{ugali}}$	155^{+19}_{-20}	50^{+8}_{-9}
TS	308.3	146.7
M_V (mag)	$-5.55^{+0.11c}_{-0.11}$	$-0.2^{+0.8c}_{-0.6}$
M_* (M_\odot)	14300^{+1800}_{-1800}	144^{+24}_{-27}
μ (mag arcsec $^{-2}$)	27.9	26.9
[Fe/H] (dex)	-1.8	-1.5
$E(B - V)$	0.124	0.113
ℓ (deg)	300.265	14.188
b (deg)	21.902	30.289
D_{GC} (kpc)	112.7	12.9
$\mu_\alpha \cos \delta$ (mas yr $^{-1}$)	$0.00^{+0.19}_{-0.18}$	$-1.7^{+0.4}_{-0.4}$
μ_δ (mas yr $^{-1}$)	$-0.46^{+0.25}_{-0.26}$	$1.6^{+0.2}_{-0.2}$
$\sum_i P_{i,\text{MM}}$	$15.0^{+1.7}_{-1.6}$	$4.2^{+1.7}_{-4.2}$

Notes. Uncertainties were derived from the highest density interval containing the peak and 68% of the marginalized posterior distribution.

^a We assume a systematic uncertainty of ± 0.1 associated with isochrone modeling.

^b The age posterior peaks at the upper bound of the allowed parameter range (13.5 Gyr); thus, we quote a lower limit at the 84% confidence level.

^c The uncertainty in M_V was calculated following Martin et al. (2008) and does not include uncertainty in the distance.

observations taken by DELVE, DECaLS (Dey et al. 2019), and DeROSITAS,⁴⁷ augmented by other DECam exposures in *griz* that were publicly available in 2019 August.⁴⁸ All exposures were processed consistently with the DES Data Management (DESDM) pipeline (Morganson et al. 2018). This pipeline enables subpercent-level photometric accuracy by calibrating based on custom-made, seasonally averaged bias and flat images and performing full-exposure sky background subtraction (Bernstein et al. 2018). The DESDM pipeline utilizes SourceExtractor and PSFEX (Bertin & Arnouts 1996; Bertin et al. 2011) for automatic source detection and photometric measurement on an exposure-level basis. We then calibrate stellar positions against *Gaia* DR2 (Gaia Collaboration et al. 2018), which provides 30 mas astrometric calibration precision. The DELVE photometry is calibrated by matching stars in each CCD to the APASS (Henden & Munari 2014) and Two Micron All Sky Survey (2MASS; Skrutskie et al. 2006) sky survey catalogs following the

⁴⁷ astro.userena.cl/derositas/

⁴⁸ Public exposures were downloaded from the Science Archive hosted by NSF's National Optical-Infrared Astronomy Research Laboratory: <http://archive1.dm.noao.edu>.

⁴⁶ <https://delve-survey.github.io>

procedure described in Drlica-Wagner et al. (2016). APASS-measured magnitudes were transformed to the DES filter system before calibration using the equations described in Appendix A4 of Drlica-Wagner et al. (2018):

$$\begin{aligned} g_{\text{DES}} &= g_{\text{APASS}} - 0.0642(g_{\text{APASS}} - r_{\text{APASS}}) - 0.0239 \\ r_{\text{DES}} &= r_{\text{APASS}} - 0.1264(r_{\text{APASS}} - i_{\text{APASS}}) - 0.0098 \\ i_{\text{DES}} &= r_{\text{APASS}} - 0.4145(r_{\text{APASS}} - J_{2\text{MASS}} - 0.81) - 0.0391, \end{aligned}$$

which have statistical rms errors per star of $\sigma_g = 0.04$ mag, $\sigma_r = 0.05$ mag, and $\sigma_i = 0.04$ mag. The relative photometric uncertainty of these derived zero points was estimated to be $\sim 3\%$ by comparing to measurements made with the DES Forward Global Calibrations Module (FGCM; Burke et al. 2018) in overlapping fields. In a small number of cases where too few stars in a given exposure were matched with the reference catalog, we derived photometric zero points from a simultaneous fit of all CCDs for that exposure.

We built a multiband catalog of unique sources by matching detections between the individual single-exposure catalogs following Drlica-Wagner et al. (2015). We started by selecting DECam exposures in the DELVE-WIDE data set with exposure times ranging from 30 to 350 s. We applied basic exposure-level cuts on the effective exposure timescale factor ($T_{\text{EFF}} > 0.3$; Neilsen et al. 2015), astrometric matching quality versus *Gaia* ($\text{ASTROMETRIC_CHI2} < 500$), and number of objects ($N_{\text{OBJECTS}} < 7.5 \times 10^5$) to remove exposures that suffered from observational, instrumental, and/or processing artifacts. To generate a unique source catalog with multiband information, we cross-matched all sources detected in individual exposures using a $1''$ matching radius. We calculated weighted-average photometric properties based on the single-exposure measurements and their associated uncertainties (Drlica-Wagner et al. 2015). In total, the data set covers approximately 6000 deg^2 in any single band, with the g and r bands providing the largest simultaneous coverage in any two bands. There are 437,373,694 unique objects in this early catalog.

Extinction from Milky Way foreground dust was calculated for each object from a bilinear interpolation to the extinction maps of Schlegel et al. (1998) and Schlafly & Finkbeiner (2011). To calculate reddening, we assumed $R_V = 3.1$ and used a set of $R_\lambda = A_\lambda / E(B - V)$ coefficients derived by DES for the g , r , and i bands, where $R_g = 3.185$, $R_r = 2.140$, and $R_i = 1.571$, respectively (DES Collaboration et al. 2018).⁴⁹ Hereafter, all quoted magnitudes are corrected for dust extinction.

3. Satellite Search

To identify Milky Way satellite candidates in the early DELVE-WIDE catalog, we applied the `simple`⁵⁰ algorithm, which has successfully been used for satellite searches on other DECam and Pan-STARRS data sets (e.g., Bechtol et al. 2015; Drlica-Wagner et al. 2019a; Mau et al. 2019). Briefly, `simple` uses an isochrone filter in the color-magnitude space of two bands to enhance the contrast of halo substructures relative to the foreground field of Milky Way stars at a given small range of distances. Because the total area covered in both the r and i bands is roughly equal for the DELVE-WIDE catalog, we

chose to run `simple` using g - and r -band data. The r band was chosen over the i band because it was found to be deeper. We note that running `simple` on g - and i -band data yields similar findings and also results in the detections of both systems presented in this paper at high significance.

Stars were selected with $|\text{SPREAD_MODEL_R}| < 0.003 + \text{SPREADERR_MODEL_R}$, where SPREAD_MODEL is a morphological variable acting as a discriminant between the best-fitting local point-spread function (PSF) model (for a point-like source) and the same PSF model but convolved with a circular exponential disk model with a scale length of one-sixteenth of the PSF's FWHM (for an extended source), and SPREADERR_MODEL is the associated error (Desai et al. 2012; DES Collaboration et al. 2018). A magnitude selection of $g < 23$ mag was applied to reduce star-galaxy confusion.

The DELVE-WIDE catalog was divided into `HEALPix` (Górski et al. 2005) pixels of $n_{\text{side}} = 32$ ($\sim 3.4 \text{ deg}^2$). For each $n_{\text{side}} = 32$ pixel, spatial overdensities of old, metal-poor stars were identified with a matched-filter isochrone, scanning in distance modulus from 16.0 to 23.0 mag in steps of 0.5 mag. Specifically, a `PARSEC` isochrone (Bressan et al. 2012) with metallicity $Z = 0.0001$ and age $\tau = 12$ Gyr was used. At each step in the distance modulus scan, stars were selected within 0.1 mag of the isochrone locus in color-magnitude space according to $\Delta(g - r) < \sqrt{0.1^2 + \sigma_g^2 + \sigma_r^2}$, where σ_g and σ_r are the photometric uncertainties on the g - and r -band magnitudes, respectively. The map of the filtered stellar density field was then smoothed by a Gaussian kernel ($\sigma = 2'$), and local density peaks were identified by iteratively raising a density threshold until fewer than 10 disconnected peaks remained above the threshold value. For each identified peak, the Poisson significance of the observed stellar counts relative to the local field density within a given aperture was computed. All peaks with Poisson significance $\text{SIG} > 5.5\sigma$ were considered for subsequent analysis.

Upon visual inspection of diagnostic plots for each of these peaks, two were identified as potential Milky Way satellite candidates, which we designate Centaurus I and DELVE 1 (Figures 1 and 2, respectively). The left two panels of Figures 1 and 2 show the filtered and smoothed stellar and galactic density fields, respectively. The middle right panels show the color-magnitude Hess diagram. The right panels show the radial distribution of isochrone-filtered stars with respect to the centroid. Note that DELVE 1 was discovered in a region of the survey with incomplete coverage, and CCD chip gaps can be seen in the upper-right region of the left panel of Figure 2.

4. Properties of the Discovered Stellar Systems

In the following subsections, we characterize the morphologies, stellar populations, distances, and proper motions of Centaurus I and DELVE 1. The most probable values of these parameters, with associated uncertainties, are presented in Table 1.

4.1. Morphological and Isochrone Parameters

We fit the morphological and isochrone parameters of Centaurus I and DELVE 1 using the maximum likelihood formulation implemented in the ultra-faint galaxy likelihood toolkit (`ugali`⁵¹; Bechtol et al. 2015; Drlica-Wagner et al. 2015, 2019a). The spatial distribution of stars was modeled with a Plummer (1911) profile, and a synthetic isochrone from

⁴⁹ An update to the DECam standard bandpasses changed these coefficients by < 1 mmag for DES DR1 (DES Collaboration et al. 2018).

⁵⁰ <https://github.com/DarkEnergySurvey/simple>

⁵¹ <https://github.com/DarkEnergySurvey/ugali>

Diagnostic Plots for Centaurus I

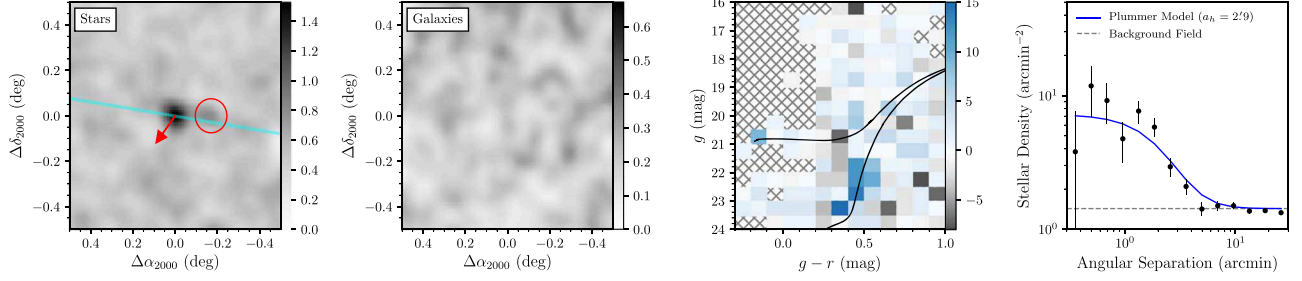


Figure 1. Source density, color–magnitude diagram, and radial density profile plots for Centaurus I. (Left) Stellar density field convolved with a Gaussian kernel of $2'$. The red arrow is drawn in the direction of the solar-reflex-corrected proper motion, and the cyan line corresponds to the great circle connecting Centaurus I and the Galactic center. A secondary overdensity near Centaurus I, which is a potential tidal feature, is circled in red. (Middle left) Background galaxy density field convolved with a Gaussian kernel of $2'$. (Middle right) Color–magnitude Hess diagram corresponding to all foreground stars within $0^\circ 10'$ of the centroid of Centaurus I minus all background stars in a concentric annulus from $0^\circ 24'$ to $0^\circ 26'$. The best-fit PARSEC isochrone (derived in Section 4.1; Table 1) is shown in black. Crosshatching indicates bins with no stars. (Right) Radial surface density profile of stars passing the isochrone filter; the errors are derived from the standard deviation of the number of stars in a given annulus divided by the area of that annulus. The blue curve corresponds to the best-fit Plummer model, assuming spherical symmetry, with $a_h = 2'9$ (derived in Section 4.1; Table 1). The dashed gray line represents the background field density.

Diagnostic Plots for DELVE 1

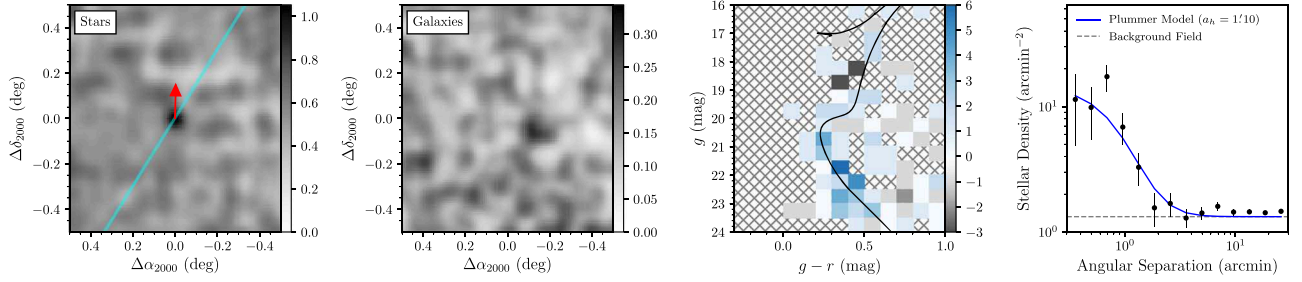


Figure 2. Similar to Figure 1, but for DELVE 1. Due to incomplete coverage in this region, CCD chip gaps (i.e., the underdense horizontal and vertical striations) are apparent in the left panel.

Bressan et al. (2012) was fit to the observed color–magnitude diagram. We simultaneously fit the R.A. and decl. (α_{2000} and δ_{2000} , respectively), extension (a_h), ellipticity (ϵ), and position angle (P.A.) of the Plummer profile, and the age (τ), metallicity (Z), and distance modulus shift ($m - M$) of the isochrone. The posterior probability distributions of each parameter were derived using an affine-invariant Markov Chain Monte Carlo ensemble sampler (emcee; Foreman-Mackey et al. 2013). Table 1 presents the best-fit parameters with uncertainties for both objects. From these properties, we derive estimates of the Galactocentric longitude and latitude (ℓ and b , respectively), the azimuthally averaged angular and physical half-light radii (r_h and $r_{1/2}$, respectively), the heliocentric distance (D_\odot), the Galactocentric distance (D_{GC} ; calculated from the three-dimensional physical separation between each object and the Galactic center, assumed to be at $R_{GC} = 8.178$ kpc; Abuter et al. 2019), the average surface brightness within one half-light radius (μ), the stellar mass integrated along the isochrone (M_*), and the metallicity ($[Fe/H]$). The *ugali* membership probability (p_{ugali}) of each star was calculated from the Poisson probabilities to detect that star based upon its spatial position, measured flux, photometric uncertainty, and the local imaging depth, given a model that includes a putative dwarf galaxy and empirical estimation of the local stellar field population. We define the sum of *ugali* membership probabilities as $\sum_i p_{i,ugali}$. Note that, due to incomplete coverage (i.e., the inhomogeneous background) in the region around DELVE 1, it is possible that our characterization of its parameters may be slightly biased. However, based on the best-fit half-light radius

and predicted Plummer profile (Figure 4), we expect that only 3 ± 2 likely member stars lie outside our covered region (compared to $\sum_i p_{i,ugali} = 50_{-9}^{+8}$ for DELVE 1).

Centaurus I was significantly detected in this likelihood analysis with a test statistic (TS) of $TS = 308.4$, corresponding to a Gaussian significance of 17.6σ (a discussion of the likelihood formalism used here is presented in Appendix C of Drlica-Wagner et al. 2019a). DELVE 1 was detected at $TS = 146.7$, or 12.1σ , which is more significant than many other satellites in DES data (Bechtol et al. 2015; Drlica-Wagner et al. 2015). We note that DELVE 1 was simultaneously discovered at a lower significance in data from Pan-STARRS PS1 (Drlica-Wagner et al. 2019a), lending confidence to the reality of this system. While Drlica-Wagner et al. (2019a) measured a smaller half-light radius, a larger absolute magnitude, and a smaller stellar mass for DELVE 1, these discrepancies are within reported uncertainties and likely explained by the difference in depth between the early DELVE-WIDE and Pan-STARRS DR1 data sets.

The spatial distributions and color–magnitude diagrams of stars in $0^\circ 5' \times 0^\circ 5'$ regions around the centroids of Centaurus I and DELVE 1 are shown in the left two panels of Figures 3 and 4, respectively. The membership probabilities for individual stars are computed using the spatial and initial mass function probabilities and isochrone selection from *ugali*. Stars with $p_{ugali} > 5\%$ are colored by their membership probability, and stars with $p_{ugali} \leq 5\%$, which are almost certainly Milky Way foreground stars, are shown in gray. The measured size and brightness suggest that Centaurus I is likely an ultra-faint

Membership Plots for Centaurus I

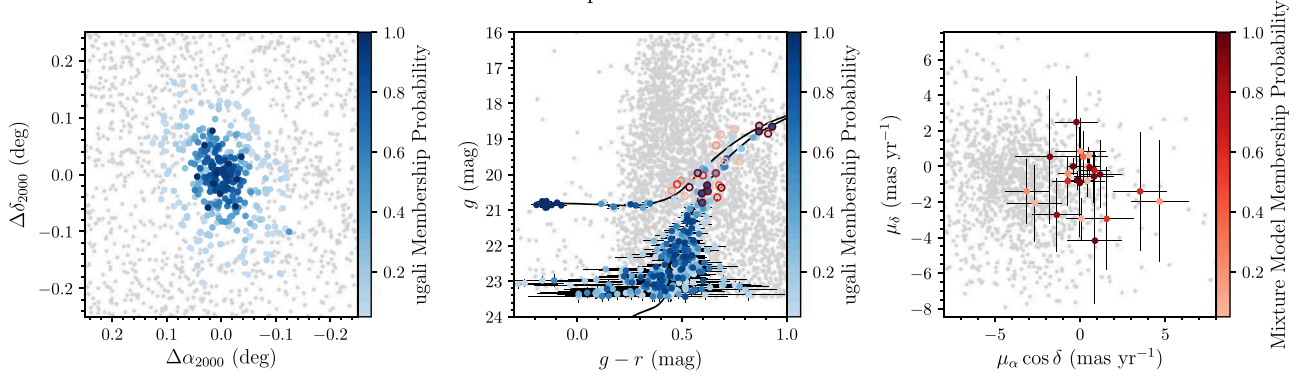


Figure 3. Spatial distribution and color–magnitude diagram plots colored by *ugali* membership probability (p_{ugali}) and proper motion plots colored by mixture model membership probability (p_{MM}) for Centaurus I. (Left) Spatial distribution of stars with $g < 23.5$ mag in a 0.25 deg^2 area region around the centroid of Centaurus I. Stars with $p_{\text{ugali}} > 0.05$ are colored by their *ugali* membership probability, and stars with $p_{\text{ugali}} \leq 0.05$ are shown in gray. (Center) Color–magnitude diagram of the stars shown in the left panel; the errors are derived from the photometric uncertainties of each band. The best-fit PARSEC isochrone (Table 1) is drawn in black. Several blue horizontal branch stars are identified as highly probable members of Centaurus I and are clustered very closely to the centroid of the system. Stars cross-matched with *Gaia* DR2 with $p_{\text{MM}} > 0.05$ are outlined by their mixture model membership probability. (Right) *Gaia* proper motions for stars cross-matched with DELVE-WIDE. Stars with $p_{\text{MM}} > 0.05$ are colored by their mixture model membership probability, and stars with $p_{\text{MM}} \leq 0.05$ are shown in gray. The *Gaia* signal for Centaurus I is distinct against the background field stars.

Membership Plots for DELVE 1

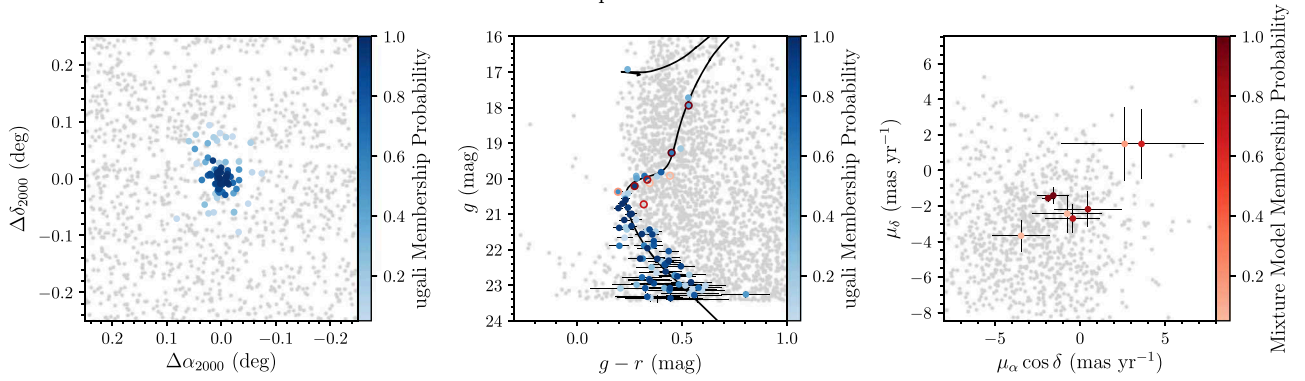


Figure 4. Similar to Figure 3, but for DELVE 1. The *Gaia* proper motion signal of DELVE 1 is marginally detected.

galaxy, while DELVE 1 is likely a faint star cluster in the Milky Way halo. Characteristics of each system are discussed in detail in Section 5.

4.2. Proper Motion

To see if stars in each system show coherent systemic motion on the sky, we cross-matched stars in the DELVE-WIDE catalog to the *Gaia* DR2 catalog (Gaia Collaboration et al. 2018) to measure their proper motions. The stellar sample was filtered by selecting stars consistent with zero parallax ($\varpi - 3\sigma_\varpi \leq 0$) and small proper motions (i.e., removing stars that would be unbound to the Milky Way if they were at the distance of a given system). Stars were selected within $1^\circ 0$ and $0^\circ 5$ for Centaurus I and DELVE 1, respectively, based on a color–magnitude selection of 0.1 mag in $g - r$ from a best-fit isochrone with metallicity $Z = 0.0002$ and age $\tau = 13.5 \text{ Gyr}$ for Centaurus I, and $Z = 0.0005$ and $\tau = 12.5 \text{ Gyr}$ for DELVE 1; this color selection was expanded to 0.2 mag for the main-sequence turnoff in DELVE 1. We note that *Gaia* DR2 has a limiting magnitude of $G \sim 21 \text{ mag}$ (Gaia Collaboration et al. 2018), which is significantly shallower than that of the DELVE-WIDE data set.

For the selected stellar sample, we applied a Gaussian mixture model to determine the proper motions of the satellite candidates

while accounting for the Milky Way foreground (Pace & Li 2019). Briefly, the mixture model separates the likelihoods of the satellite and the Milky Way stars, decomposing each into a product of spatial and proper motion likelihoods. Stars that are closer to the centroid are given higher weight by assuming the best-fit projected Plummer profile (from Section 4.1), and stars well outside the satellite help determine the Milky Way foreground proper motion distribution. The MultiNest algorithm (Feroz & Hobson 2008; Feroz et al. 2009) was used to determine the best-fit parameters, including the proper motions of the satellite and of the Milky Way foreground stars. The mixture model membership probability (p_{MM}) of each star was calculated by taking the ratio of the satellite likelihood to the total likelihood from the posterior distribution (see Pace & Li 2019 for more details).

We derive a proper motion for Centaurus I of $(\mu_\alpha \cos \delta, \mu_\delta) = (0.00^{+0.19}_{-0.18}, -0.46^{+0.25}_{-0.26}) \text{ mas yr}^{-1}$ (Table 1, right panel of Figure 3) and a proper motion for DELVE 1 of $(\mu_\alpha \cos \delta, \mu_\delta) = (-1.7^{+0.4}_{-0.4}, 1.6^{+0.2}_{-0.2}) \text{ mas yr}^{-1}$ (Table 1, right panel of Figure 4). In the right panels of Figures 3 and 4, stars with $p_{\text{MM}} > 5\%$ are colored by their membership probability, and stars with $p_{\text{MM}} \leq 5\%$, which are almost certainly Milky Way foreground stars, are shown in gray. Stars cross-matched between DELVE-WIDE and *Gaia* DR2 with $p_{\text{MM}} > 5\%$ are outlined in the center

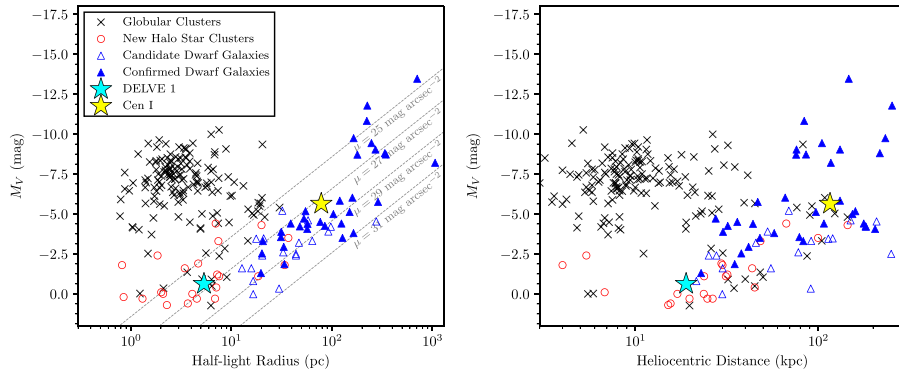


Figure 5. (Left) Absolute magnitude vs. azimuthally averaged physical half-light radius of Milky Way dwarf galaxy satellites (unfilled and filled blue triangles for candidate and confirmed dwarf galaxies, respectively; Drlica-Wagner et al. 2019a, and references therein), globular clusters (black crosses; Harris 1996), and recently discovered Milky Way halo star clusters (unfilled red circles; Fadelly et al. 2011; Muñoz et al. 2012; Balbinot et al. 2013; Belokurov et al. 2014; Laevens et al. 2014, 2015b; Kim & Jerjen 2015b; Kim et al. 2016; Luque et al. 2016, 2017, 2018; Koposov et al. 2017; Mau et al. 2019; Torrealba et al. 2019). Centaurus I is shown as a yellow star, and DELVE 1 is shown as a cyan star. Lines of constant surface brightness are drawn as dashed gray lines. (Right) Absolute magnitude vs. heliocentric distance of stellar systems in orbit around the Milky Way. Centaurus I occupies a position in this three-dimensional parameter space consistent with the population of ultra-faint galaxy satellites of the Milky Way, while the small physical size and heliocentric distance of DELVE 1 are more consistent with those of faint halo star clusters.

panels of Figures 3 and 4. We define the sum of the mixture model membership probabilities as $\sum_i p_{i,MM}$. We find $\sum_i p_{i,MM} = 15.0^{+1.7}_{-1.6}$ and $\sum_i p_{i,MM} = 4.2^{+1.7}_{-4.2}$ for members with proper motions consistent with Centaurus I and DELVE 1, respectively.

Based on the posterior distributions, number of stars, and diagnostic plots, we clearly detect the proper motion of Centaurus I, helping confirm that it is a real system. While we do not find enough member stars to robustly disentangle the proper motion of DELVE 1 from the Milky Way foreground, the lack of a clear proper motion detection in *Gaia* DR2 for DELVE 1 does not disqualify it as a real stellar system. Importantly, *Gaia* DR2 has a limiting magnitude of $G \sim 21$ mag (Gaia Collaboration et al. 2018), while the most probable member stars of DELVE 1 are old main-sequence stars fainter than $G \sim 21$ mag, according to the *ugal*i analysis. If we assume that DELVE 1 has a Chabrier (2001) initial mass function with an age of 12.5 Gyr and $[\text{Fe}/\text{H}]$ of -1.5 dex, then we predict that we should observe $N = 6 \pm 3$ stars brighter than $G \sim 21$ mag based on 1000 *ugal*i simulations. Performing a similar calculation for Centaurus I with an age of 13.5 Gyr and $[\text{Fe}/\text{H}]$ of -1.8 dex, we predict that we should observe $N = 22 \pm 5$ stars. Given the small number of predicted members accessible at these brighter magnitudes, it is unsurprising that there is no clear proper motion signal for DELVE 1, which has far fewer likely member stars than Centaurus I, in *Gaia* DR2.

5. Discussion

We have presented the discovery of two new stellar systems and characterized their morphology, stellar age and metallicity, distance, and kinematics. These measurements can provide insight into their likely natures as a dark-matter-dominated faint dwarf galaxy satellite and a faint halo star cluster, respectively.

The left panel of Figure 5 presents the distribution of Milky Way dwarf galaxy satellites (unfilled and filled blue triangles), Milky Way halo star clusters (unfilled red circles), and globular clusters (black crosses) in size–luminosity space, and the right panel of Figure 5 shows the same satellites in distance–luminosity space. Based on their positions in Figure 5, Centaurus I appears to have properties that are consistent with the population of known dwarf galaxy satellites of the Milky Way (e.g., its properties are

similar to those of Leo IV), and DELVE 1 appears to have properties that are consistent with the population of known halo star clusters of the Milky Way (e.g., its properties are similar to those of Muñoz 1). However, further investigations will be needed to confirm these classifications. The derived properties of each object are discussed in detail in the following subsections.

5.1. Centaurus I

We found that Centaurus I is an old ($\tau > 12.85$ Gyr), extended ($r_{1/2} = 79^{+14}_{-10}$ pc), and faint ($M_V = -5.55^{+0.11}_{-0.11}$ mag) stellar system with an average systemic metallicity ($[\text{Fe}/\text{H}] = -1.8$ dex) consistent with that of most ultra-faint galaxies (McConnachie 2012, 2019 edition). Given its physical size, Centaurus I is relatively bright compared to the population of ultra-faint galaxies with similar size, but its absolute magnitude and physical size are consistent with the definition for ultra-faint galaxies put forth in Simon (2019), i.e., a dwarf galaxy with $M_V \gtrsim -7.7$ mag.

The well-populated horizontal branch of Centaurus I makes it an excellent candidate for RR Lyrae star searches. In particular, Equation (4) of Martínez-Vázquez et al. (2019) predicts that a system with $M_V = -5.55$ mag should have $\gtrsim 6$ RR Lyrae stars. Discovering RR Lyrae stars in Centaurus I would aid in verifying the nature of this system by allowing for the determination of its physical properties with greater precision (e.g., Greco et al. 2008; Garofalo et al. 2013; Vivas et al. 2016; Ferguson & Strigari 2019).

Investigation of the region around Centaurus I reveals a secondary, less significant overdensity displaced ~ 0.17 to the west of Centaurus I (red circle in Figure 1). This elongated overdensity near the centroid of Centaurus I could be a candidate tidal feature of the system. Such potentially tidally disrupted structures have previously been observed in some Milky Way satellites (e.g., Sand et al. 2009, 2012; Muñoz et al. 2010; Roderick et al. 2015) and provide clues to investigating the dynamical state of these systems (e.g., Piatek & Pryor 1995; Deason et al. 2012; Lokas et al. 2012; Collins et al. 2017). For instance, the fact that the tidal tails in Tucana III show a high velocity gradient, but no significant density variation, suggests that it is on radial orbit and had a recent close pericentric passage about the Milky Way (Drlica-Wagner et al. 2015; Li et al. 2018).

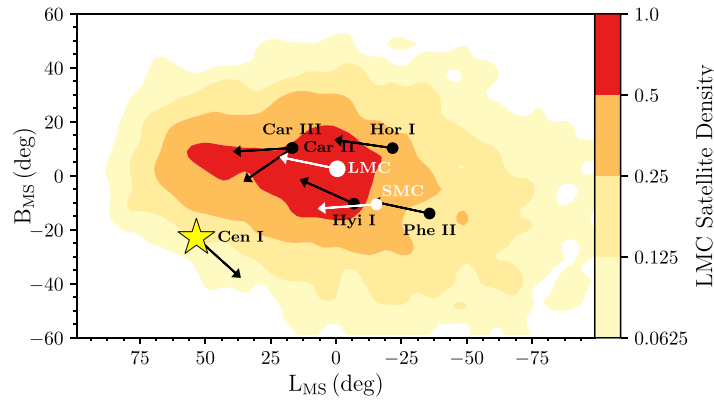


Figure 6. Relative density of simulated LMC satellites from Jethwa et al. (2016) normalized to unity. Centaurus I is shown as a yellow star, and five likely LMC satellites (Hor I, Car II, Car III, Hyi I, Phe II; Kallivayalil et al. 2018; Erkal & Belokurov 2019) are shown as black circles; the LMC and SMC are shown as white circles. Arrows indicate the solar-reflex-corrected proper motions of each system (no physical meaning is attributed to the magnitudes of these arrows). Note that Car II and Car III are spatially coincident but have different proper motion vectors. The motion and position of Centaurus I are opposite to those of the LMC and its satellites, making an association unlikely. DELVE 1 does not appear because it is located at $(L_{\text{MS}}, B_{\text{MS}}) = (135^\circ, -67^\circ)$.

This radial orbit is confirmed by dynamical modeling (Erkal et al. 2018) and proper motion measurements from *Gaia* DR2 (Simon 2018).

However, this might not be the case for Centaurus I. Even if a very eccentric orbit is assumed for Centaurus I, its current location is too far from the center of the Milky Way to maintain features induced by tidal stripping after a close pericenter (e.g., Peñarrubia et al. 2008; Kazantzidis et al. 2011; Barber et al. 2015). Tidal structures induced during the pericentric passage seem to be short-lived and are expected to fade out while traveling to the apocenter. According to Li et al. (2018), circumstantial morphological properties alone cannot provide reliable evidence for tidal features. We also note that the displacement of the secondary overdensity is not aligned with the solar-reflex-corrected proper motion of Centaurus I; this is reminiscent of the Hercules ultra-faint galaxy, which exhibits elongated and irregular morphology perpendicular to a very eccentric orbit at a heliocentric distance of 140 kpc (Küpper et al. 2017). Garling et al. (2018) used observations of RR Lyrae variable stars to determine that much of the stellar content of Hercules has been stripped, with its orbit aligned along its minor axis. Other recent studies have been inconclusive about whether or not Hercules has undergone tidal stripping (Fu et al. 2019). In addition, follow-up deep imaging has shown that candidate tidal features identified in relatively shallow imaging surveys can actually be artifacts caused by clumps of Milky Way foreground and background stars (e.g., Leo V; Mutlu-Pakdil et al. 2019). Given that the secondary overdensity appears to be disconnected from the centroid of Centaurus I (Figure 1), it is also conceivable that it is an associated companion (e.g., as with Car II and Car III; Torrealba et al. 2018). Thus, follow-up deep imaging and spectroscopic studies of the candidate tidal features of Centaurus I are needed to illuminate their structure and determine whether this secondary overdensity is indeed physically associated with Centaurus I.

It is also interesting to consider the possible origins of Centaurus I. DES has revealed a concentration of Milky Way ultra-faint galaxy satellites around the Large and Small Magellanic Clouds (the LMC and SMC, respectively), suggesting that the LMC has brought its own satellite population into the Milky Way (e.g., D’Onghia & Lake 2008; Deason et al. 2015; Sales et al. 2017; Jethwa et al. 2018; Kallivayalil et al. 2018; Erkal & Belokurov 2019; Jahn et al. 2019; Nadler et al. 2019c). Hence, we consider whether or not Centaurus I is

associated with the LMC, given their relatively small angular separation ($\sim 58^\circ$). To investigate the potential association of Centaurus I with the LMC, we present the spatial position and solar-reflex-corrected proper motion vector of Centaurus I over simulated LMC tidal debris from Jethwa et al. (2016) in Magellanic Stream coordinates (Nidever et al. 2008) along with the LMC, SMC, and five other ultra-faint galaxies associated with the LMC in Figure 6. These five ultra-faint galaxies are Horologium I, Carina II, Carina III, Hydrus I, and Phoenix II (Kallivayalil et al. 2018; Erkal & Belokurov 2019), with proper motion measurements coming from Kallivayalil et al. (2018) and Pace & Li (2019). While Pardy et al. (2020) suggested that Carina and Fornax are satellites of the LMC, orbit modeling done by Erkal & Belokurov (2019) found that neither Carina nor Fornax are likely LMC satellites; hence, we do not include these systems in Figure 6. The position of Centaurus I is only marginally consistent with that of the simulated LMC satellites, and its proper motion is nearly antiparallel to that of the LMC and its probable satellites. Thus, we find no strong evidence in support of Centaurus I being a satellite of the LMC from this analysis.

Erkal & Belokurov (2019) put forward an alternative technique for determining LMC membership where the orbit of each satellite is rewound in the presence of the Milky Way and LMC to determine if they were bound to the LMC before it fell onto the Milky Way. Erkal & Belokurov (2019) also used this technique on satellites without radial velocity measurements to determine if there were any radial velocities for which the satellites belonged to the LMC. This is done by sampling the proper motions and distances from their observed uncertainties while sampling the radial velocity uniformly from -500 to 500 km s^{-1} . This sampling was done 100,000 times, and, for each realization, we rewound Centaurus I in the combined presence of the LMC and the Milky Way for 5 Gyr to determine whether it was originally bound to the LMC. In this analysis, we model the LMC as a Hernquist profile (Hernquist 1990) with a mass of $1.5 \times 10^{11} M_\odot$ and a scale radius of 17.13 kpc, consistent with recent measurements of the LMC mass (Peñarrubia et al. 2016; Erkal et al. 2019). With this analysis, we find that, for radial velocities between 350 and 410 km s^{-1} , Centaurus I has a $>5\%$ chance of being an LMC satellite with a maximum probability of $\sim 10\%$ at a radial velocity of 385 km s^{-1} . While this probability is still small, if the radial velocity is found to be in this range, it would warrant

additional investigation. Outside of this range, the probability quickly drops below 1% for radial velocities below $\sim 300 \text{ km s}^{-1}$ and above 490 km s^{-1} . We also note that future proper motion measurements with *Gaia* DR3 will improve the proper motion uncertainties and thus give a more accurate trajectory when rewinding the orbit of Centaurus I.

We also consider whether Centaurus I is associated with the Vast Polar Structure (VPOS) of the Milky Way (Pawlowski et al. 2012). A large fraction of Milky Way satellite galaxies have recently been determined (Fritz et al. 2018) to lie on a thin, corotating plane nearly perpendicular to the Milky Way’s stellar disk (Pawlowski & Kroupa 2013, 2020). Adopting the same VPOS parameters as Fritz et al. (2018), namely the assumed normal $(l_{\text{MW}}, b_{\text{MW}}) = (169.3, -2.8) \text{ deg}$ and angular tolerance $\theta_{\text{inVPOS}} = 36.87^\circ$, we find it unlikely that Centaurus I is a VPOS member. Specifically, the minimum possible angle between the VPOS and the satellite’s orbital pole based on spatial information alone is $\theta_{\text{pred}} = 35.15^\circ$, while the probability that the orbital pole lies within θ_{inVPOS} of the VPOS normal ranges from $\sim 4\%$ to 10% depending on the assumed heliocentric radial velocity. In addition, the available spatial and proper motion measurements prefer a counter-orbiting orientation relative to the VPOS. However, we note that the orbital inconsistency does not rule out the possibility of Centaurus I being a VPOS member as this analysis is based on the limited information currently available. A radial velocity measurement is required to conclusively categorize Centaurus I as either a VPOS member or not and to determine whether or not it is co- or counter-orbiting.

5.2. DELVE 1

We identified DELVE 1 as a faint ($M_V = -0.2^{+0.8}_{-0.6} \text{ mag}$), compact ($r_{1/2} = 5.4^{+1.5}_{-1.1} \text{ pc}$), and low-mass ($M_* = 144^{+24}_{-27} M_\odot$) stellar system located at a relatively close heliocentric distance ($D_\odot = 19.0^{+0.5}_{-0.6} \text{ kpc}$). As such, it appears to be consistent with the population of faint halo star clusters of the Milky Way discovered in recent years (e.g., Fadelly et al. 2011; Muñoz et al. 2012; Balbinot et al. 2013; Belokurov et al. 2014; Laevens et al. 2014; Kim & Jerjen 2015b; Laevens et al. 2015b; Kim et al. 2016; Luque et al. 2016, 2017; Koposov et al. 2017; Luque et al. 2018; Mau et al. 2019; Torrealba et al. 2019).

These faint halo clusters have been proposed to be the remnants of merger events—they were accreted onto the Milky Way along with their host galaxies, but the host galaxies themselves were disrupted due to the Milky Way tides (e.g., Searle & Zinn 1978; Gnedin & Ostriker 1997; Koposov et al. 2007; Forbes & Bridges 2010; Leaman et al. 2013; Massari et al. 2017). Specifically, the compactness of these star clusters is essential to longer survival timescales despite the strong tidal fields during merging processes, while the host galaxies of these clusters are disrupted by the Milky Way tides on shorter timescales. This scenario has received considerable observational support from the age, metallicity, and spatial distributions of these clusters (e.g., Zinn 1993; Da Costa & Armandroff 1995; Mackey & Gilmore 2004; Marín-Franch et al. 2009; Dotter et al. 2010; Mackey et al. 2010; Keller et al. 2011) and is further supported by the close resemblance between Milky Way halo clusters and the clusters thought to have been accreted with the dwarf galaxies that fell into the Milky Way (e.g., Smith et al. 1998; Johnson et al. 1999; Da Costa 2003; Wetzel et al. 2015; Yozin & Bekki 2015; Bianchini et al. 2017). Meanwhile, with the advent of *Gaia*, the assembly history of the Milky Way has been revealed in greater detail, shedding light on the origin of these systems. Recently, kinematic data from *Gaia* have been

used to propose that $\sim 35\%$ of the Milky Way globular clusters were accreted with merger events (Massari et al. 2019). In addition, Kruijssen et al. (2019) suggested that $\sim 40\%$ of the Milky Way globular clusters formed ex situ and accreted through merger events based on analysis of the age–metallicity distributions of the globular clusters. This proposal has been supported by a chemical abundance analysis of Palomar 13, which found possible similarities between Palomar 13 and other globular clusters that purportedly accreted through either the *Gaia*-Enceladus or Sequoia events (Koch & Côté 2019).

Although DELVE 1 does not have spectroscopically measured metallicity or radial velocity, it is possible to consider whether DELVE 1 was accreted with the LMC, which is known to have brought a large population of star clusters (Bica et al. 2008). The age and metallicity of DELVE 1 are consistent with those found in the LMC star clusters; however, the position of DELVE 1 in the sky easily rules out its association with the LMC, even if the leading arm of the MC (a very extended H I gas structure) is taken into account (Nidever et al. 2010). It is important to note that, without spectroscopic information, we are unable to draw a robust conclusion on the origin of DELVE 1.

Exploring the long-term dynamical evolution of DELVE 1 may also provide insights into its origins. To estimate its survival timescale in its current evolutionary state, we compute the evaporation timescale (i.e., the time over which stars in a star cluster escape the system due to two-body relaxation) following Koposov et al. (2007). Specifically, we compute $t_{\text{ev}} \simeq 12t_{\text{th}}$ (Koposov et al. 2007), where t_{th} is the half-mass relaxation time given by Equation (7.2) of Meylan & Heggie (1997):

$$t_{\text{th}} = 0.138 \frac{M^{1/2} R_h^{3/2}}{\langle m \rangle G^{1/2} \ln \Lambda},$$

where M is the total stellar mass of the cluster, R_h is the half-mass–radius (we assume $R_h \sim r_{1/2}$), $\langle m \rangle$ is the mean stellar mass of stars in the cluster, G is the gravitational constant, and $\Lambda \simeq 0.4N$, where N is the total number of stars in the cluster (a richness of 610 was fit to DELVE 1 with *ugal*). We find $t_{\text{ev}} = 3 \text{ Gyr}$ for DELVE 1, which is longer than that of both Kop 1 and Kop 2 (0.7 Gyr and 1.1 Gyr, respectively; Koposov et al. 2007). However, this evaporation timescale is still only a quarter of the estimated lifetime of the star cluster ($\tau = 12.5 \text{ Gyr}$), suggesting that DELVE 1 cannot have persisted in its observed structural and dynamic state throughout its lifetime.

5.3. Classification of Ultra-faint Objects

As noted above, the physical classifications of Centaurus I and DELVE 1 are uncertain without spectroscopic information. Classifications based on physical size and absolute magnitude have become less certain as surveys have revealed a continuum of objects located between the size–luminosity loci of classical dwarf galaxies and globular clusters. In particular, the classification of systems with $M_V > -2 \text{ mag}$ and $10 \text{ pc} \lesssim r_{1/2} \lesssim 40 \text{ pc}$ is uncertain, leading authors to call this region of parameter space the “valley of ambiguity” (Gilmore et al. 2007; Conn et al. 2018a, 2018b).

While both Centaurus I and DELVE 1 reside outside the most ambiguous region of parameter space, definitive classification rests on the determination of the dynamical mass by measuring the velocity dispersion. Generally, for an ultra-faint satellite, a resolved velocity dispersion implies the presence of a dark matter halo and,

definitionally, a classification as a dwarf galaxy (Willman & Strader 2012). However, despite significant investment of telescope time, observations of many recently discovered systems lack sufficient statistical and systematic precision to resolve a velocity dispersion smaller than a few km s^{-1} (e.g., Simon 2019). Many newly discovered Milky Way satellites still lack clear velocity and/or metallicity dispersion measurements (Kirby et al. 2015, 2017; Martin et al. 2016a, 2016b; Walker et al. 2016; Simon et al. 2017), making it difficult to reliably categorize them as either faint star clusters or ultra-faint dwarfs. This has led to the adoption of other indirect arguments to infer the presence of a dark matter halo, including large metallicity dispersions (Simon et al. 2011; Willman & Strader 2012), lack of light element correlations (e.g., in Tucana III; Marshall et al. 2019), and/or low neutron-capture element abundances (Ji et al. 2019). These indirect classification criteria are founded on the argument that only systems with a dark matter halo are able to retain and self-enrich their gas after the initial episodes of star formation (e.g., Kirby et al. 2013) and generally rely on the lack of star clusters with these observed properties. However, even metallicity arguments are challenging when there are few member stars that are bright enough for spectroscopic follow-up with current facilities.

The classification challenge will become more pressing in the coming decade with the advent of the Large Synoptic Survey Telescope (LSST), which is expected to discover up to several hundred new ultra-faint galaxy candidates and an as-of-yet unpredicted number of faint halo star clusters (Drlica-Wagner et al. 2019b). Upcoming 30 m telescopes will provide access to the spectra of fainter member stars, but instrument stability will likely still be a driving limitation in resolving the small velocity dispersions expected in these systems. Understanding how to classify new ultra-faint stellar systems will thus be an important and challenging issue in the era of LSST, particularly when using the population demographics of the Milky Way ultra-faint galaxies as a probe of dark matter microphysics. In the end, even with all available information, it still may only be possible to make probabilistic classifications of these systems, which can be folded into studies of the Milky Way ultra-faint galaxy population as a systematic uncertainty.

6. Summary

We present the discovery of two ultra-faint stellar systems, Centaurus I and DELVE 1, in early data from the DELVE survey. These stellar systems were the most significant new stellar overdensities detected in an automated search of $\sim 6000 \text{ deg}^2$ in the southern hemisphere. Based on morphological and isochrone modeling, we tentatively classify Centaurus I as an ultra-faint galaxy and DELVE 1 as a faint halo star cluster. Using proper motions from *Gaia* DR2, we confirmed that both of these systems appear to be physically bound associations of stars with coherent motion on the sky. We also found that neither of these satellites is likely to be associated with the LMC and that Centaurus I is unlikely to be associated with the VPOS. Given these two discoveries in the early DELVE-WIDE data and predictions from numerical simulations (e.g., Nadler et al. 2018), we anticipate that DELVE will discover ~ 10 satellite galaxies as it continues to complete contiguous DECam coverage of the southern sky. Furthermore, Nadler et al. (2019c) predicted that ~ 100 satellites of the Milky Way with $M_V < 0 \text{ mag}$ and $r_{1/2} > 10 \text{ pc}$ still remain to be discovered, and DECam surveys like DELVE will play an important role in advancing this census.

S.M. is supported by the University of Chicago Provost’s Scholar Award. A.B.P. acknowledges support from NSF grant AST-1813881. J.L.C. acknowledges support from NSF grant AST-1816196. Research by D.J.S. is supported by NSF grants AST-1821987, AST-1821967, AST-1813708, AST-1813466, and AST-1908972. A.M. acknowledges support from CONICYT FONDECYT Regular grant 1181797. This project is partially supported by the NASA Fermi Guest Investigator Program Cycle 9 No. 91201. This work is partially supported by Fermilab LDRD project L2019-011.

This project used data obtained with the Dark Energy Camera (DECam), which was constructed by the Dark Energy Survey (DES) collaboration. Funding for the DES Projects has been provided by the DOE and NSF (USA), MISE (Spain), STFC (UK), HEFCE (UK), NCSA (UIUC), KICP (U. Chicago), CCAPP (Ohio State), MIFPA (Texas A&M University), CNPQ, FAPERJ, FINEP (Brazil), MINECO (Spain), DFG (Germany), and the collaborating institutions in the Dark Energy Survey, which are Argonne Lab, UC Santa Cruz, University of Cambridge, CIEMAT-Madrid, University of Chicago, University College London, DES-Brazil Consortium, University of Edinburgh, ETH Zürich, Fermilab, University of Illinois, ICE (IEEC-CSIC), IFAE Barcelona, Lawrence Berkeley Lab, LMU München, and the associated Excellence Cluster Universe, University of Michigan, NSF’s National Optical-Infrared Astronomy Research Laboratory, University of Nottingham, Ohio State University, OzDES Membership Consortium University of Pennsylvania, University of Portsmouth, SLAC National Lab, Stanford University, University of Sussex, and Texas A&M University.

This work has made use of data from the European Space Agency (ESA) mission *Gaia* (<https://www.cosmos.esa.int/gaia>), processed by the *Gaia* Data Processing and Analysis Consortium (DPAC, <https://www.cosmos.esa.int/web/gaia/dpac/consortium>). Funding for the DPAC has been provided by national institutions, in particular the institutions participating in the *Gaia* Multilateral Agreement.

Based on observations at Cerro Tololo Inter-American Observatory, NSF’s National Optical-Infrared Astronomy Research Laboratory (2019A-0305; PI: Drlica-Wagner), which is operated by the Association of Universities for Research in Astronomy (AURA) under a cooperative agreement with the National Science Foundation.

This manuscript has been authored by Fermi Research Alliance, LLC, under contract No. DE-AC02-07CH11359 with the US Department of Energy, Office of Science, Office of High Energy Physics. The United States Government retains and the publisher, by accepting the article for publication, acknowledges that the United States Government retains a non-exclusive, paid-up, irrevocable, worldwide license to publish or reproduce the published form of this manuscript, or allow others to do so, for United States Government purposes.

Facilities: Blanco, *Gaia*.

Software: *astropy* (Astropy Collaboration et al. 2013; Price-Whelan et al. 2018), *emcee* (Foreman-Mackey et al. 2013), *fitsio*,⁵² *HEALPix* (Górski et al. 2005),⁵³ *healpy*,⁵⁴ *Matplotlib* (Hunter 2007), *numpy* (Van Der Walt et al. 2011), *scipy* (Jones et al. 2001), *ugali* (Bechtol et al. 2015).⁵⁵

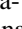

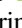

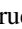
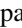


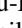
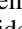
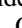
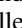



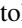


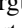
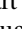
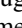
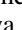
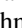

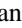
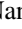

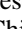

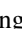
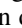





⁵² <https://github.com/esheldon/fitsio>

⁵³ <http://healpix.sourceforge.net>

⁵⁴ <https://github.com/healpy/healpy>

⁵⁵ <https://github.com/DarkEnergySurvey/ugali>

ORCID iDs

S. Mau  <https://orcid.org/0000-0003-3519-4004>
W. Cerny  <https://orcid.org/0000-0003-1697-7062>
A. B. Pace  <https://orcid.org/0000-0002-6021-8760>
Y. Choi  <https://orcid.org/0000-0003-1680-1884>
A. Drlica-Wagner  <https://orcid.org/0000-0001-8251-933X>
L. Santana-Silva  <https://orcid.org/0000-0003-3402-6164>
A. H. Riley  <https://orcid.org/0000-0001-5805-5766>
D. Erkal  <https://orcid.org/0000-0002-8448-5505>
G. S. Stringfellow  <https://orcid.org/0000-0003-1479-3059>
M. Adamów  <https://orcid.org/0000-0002-6904-359X>
J. L. Carlin  <https://orcid.org/0000-0002-3936-9628>
R. A. Gruendl  <https://orcid.org/0000-0002-4588-6517>
N. Kuropatkin  <https://orcid.org/0000-0003-2511-0946>
T. S. Li  <https://orcid.org/0000-0002-9110-6163>
C. E. Martínez-Vázquez  <https://orcid.org/0000-0002-9144-7726>
B. Mutlu-Pakdil  <https://orcid.org/0000-0001-9649-4815>
E. H. Neilsen  <https://orcid.org/0000-0002-7357-0317>
D. L. Nidever  <https://orcid.org/0000-0002-1793-3689>
K. A. G. Olsen  <https://orcid.org/0000-0002-7134-8296>
D. J. Sand  <https://orcid.org/0000-0003-4102-380X>
E. J. Tollerud  <https://orcid.org/0000-0002-9599-310X>
B. Yanny  <https://orcid.org/0000-0002-9541-2678>
S. Allam  <https://orcid.org/0000-0002-7069-7857>
W. A. Barkhouse  <https://orcid.org/0000-0001-5547-3938>
K. Bechtol  <https://orcid.org/0000-0001-8156-0429>
E. F. Bell  <https://orcid.org/0000-0002-5564-9873>
P. Balaji  <https://orcid.org/0000-0002-8462-048X>
D. Crnojević  <https://orcid.org/0000-0002-1763-4128>
P. S. Ferguson  <https://orcid.org/0000-0001-6957-1627>
C. Gallart  <https://orcid.org/0000-0001-6728-806X>
A. K. Hughes  <https://orcid.org/0000-0002-1718-0402>
D. J. James  <https://orcid.org/0000-0001-5160-4486>
P. Jethwa  <https://orcid.org/0000-0003-0010-8129>
L. C. Johnson  <https://orcid.org/0000-0001-6421-0953>
K. Kuehn  <https://orcid.org/0000-0003-0120-0808>
S. Majewski  <https://orcid.org/0000-0003-2025-3147>
Y.-Y. Mao  <https://orcid.org/0000-0002-1200-0820>
P. Massana  <https://orcid.org/0000-0002-8093-7471>
M. McNanna  <https://orcid.org/0000-0001-5435-7820>
A. Monachesi  <https://orcid.org/0000-0003-2325-9616>
E. O. Nadler  <https://orcid.org/0000-0002-1182-3825>
N. E. D. Noël  <https://orcid.org/0000-0002-8282-469X>
A. Palmese  <https://orcid.org/0000-0002-6011-0530>
F. Paz-Chinchon  <https://orcid.org/0000-0003-1339-2683>
A. Pieres  <https://orcid.org/0000-0001-9186-6042>
N. Shipp  <https://orcid.org/0000-0003-2497-091X>
M. Soares-Santos  <https://orcid.org/0000-0001-6082-8529>
K. Tavangar  <https://orcid.org/0000-0001-6584-6144>
R. P. van der Marel  <https://orcid.org/0000-0001-7827-7825>
A. K. Vivas  <https://orcid.org/0000-0003-4341-6172>
A. R. Walker  <https://orcid.org/0000-0002-7123-8943>
R. H. Wechsler  <https://orcid.org/0000-0003-2229-011X>

References

Aaronson, M. 1983, *ApJL*, 266, L11
Abuter, R., Amorim, A., Bauböck, M., et al. 2019, *A&A*, 625, L10
Albert, A., Anderson, B., Bechtol, K., et al. 2017, *ApJ*, 834, 110
Astropy Collaboration, Robitaille, T. P., Tollerud, E. J., et al. 2013, *A&A*, 558, A33
Balbinot, E., Santiago, B. X., da Costa, L., et al. 2013, *ApJ*, 767, 101

Barber, C., Starkenburg, E., Navarro, J. F., & McConnachie, A. W. 2015, *MNRAS*, 447, 1112
Bechtol, K., Drlica-Wagner, A., Balbinot, E., et al. 2015, *ApJ*, 807, 50
Belokurov, V., Irwin, M. J., Koposov, S. E., et al. 2014, *MNRAS*, 441, 2124
Belokurov, V., Walker, M. G., Evans, N. W., et al. 2009, *MNRAS*, 397, 1748
Belokurov, V., Walker, M. G., Evans, N. W., et al. 2010, *ApJL*, 712, L103
Belokurov, V., Zucker, D. B., Evans, N. W., et al. 2006, *ApJL*, 647, L111
Belokurov, V., Zucker, D. B., Evans, N. W., et al. 2007, *ApJ*, 654, 897
Bernstein, G. M., Abbott, T. M. C., Armstrong, R., et al. 2018, *PASP*, 130, 054501
Bertin, E. 2011, in ASP Conf. Ser. 442, *Astronomical Data Analysis Software and Systems XX*, ed. I. N. Evans et al. (San Francisco, CA: ASP), 435
Bertin, E., & Arnouts, S. 1996, *A&AS*, 117, 393
Bianchini, P., Sills, A., & Miholics, M. 2017, *MNRAS*, 471, 1181
Bica, E., Bonatto, C., Dutra, C. M., & Santos, J. F. C. 2008, *MNRAS*, 389, 678
Boylan-Kolchin, M., Weisz, D. R., Johnson, B. D., et al. 2015, *MNRAS*, 453, 1503
Bressan, A., Marigo, P., Girardi, L., et al. 2012, *MNRAS*, 427, 127
Burke, D. L., Rykoff, E. S., Allam, S., et al. 2018, *AJ*, 155, 41
Carlin, J. L., Sand, D. J., Price, P., et al. 2016, *ApJL*, 828, L5
Chabrier, G. 2001, *ApJ*, 554, 1274
Collins, M. L. M., Tollerud, E. J., Sand, D. J., et al. 2017, *MNRAS*, 467, 573
Conn, B. C., Jerjen, H., Kim, D., & Schirmer, M. 2018a, *ApJ*, 852, 68
Conn, B. C., Jerjen, H., Kim, D., & Schirmer, M. 2018b, *ApJ*, 857, 70
Da Costa, G. S. 2003, in ASP Conf. Ser. 296, *New Horizons in Globular Cluster Astronomy*, ed. G. Piotto et al. (San Francisco, CA: ASP), 545
Da Costa, G. S., & Armandroff, T. E. 1995, *AJ*, 109, 2533
Deason, A. J., Belokurov, V., Evans, N. W., Watkins, L. L., & Fellhauer, M. 2012, *MNRAS*, 425, L101
Deason, A. J., Wetzel, A. R., Garrison-Kimmel, S., & Belokurov, V. 2015, *MNRAS*, 453, 3568
Desai, S., Armstrong, R., Mohr, J. J., et al. 2012, *ApJ*, 757, 83
DES Collaboration, Abbott, T. M. C., Abdalla, F. B., et al. 2018, *ApJS*, 239, 18
Dey, A., Schlegel, D. J., Lang, D., et al. 2019, *AJ*, 157, 168
D'Onghia, E., & Lake, G. 2008, *ApJL*, 686, L61
Dotter, A., Sarajedini, A., Anderson, J., et al. 2010, *ApJ*, 708, 698
Drlica-Wagner, A., Bechtol, K., Allam, S., et al. 2016, *ApJL*, 833, L5
Drlica-Wagner, A., Bechtol, K., Mau, S., et al. 2019a, *ApJ*, submitted (arXiv:1912.03302)
Drlica-Wagner, A., Bechtol, K., Rykoff, E. S., et al. 2015, *ApJ*, 813, 109
Drlica-Wagner, A., Mao, Y.-Y., Adhikari, S., et al. 2019b, arXiv:1902.01055
Drlica-Wagner, A., Sevilla-Noarbe, I., Rykoff, E. S., et al. 2018, *ApJS*, 235, 33
Erkal, D., Belokurov, V., Laporte, C. F. P., et al. 2019, *MNRAS*, 487, 2685
Erkal, D., & Belokurov, V. A. 2019, *MNRAS*, submitted (arXiv:1907.09484)
Erkal, D., Li, T. S., Koposov, S. E., et al. 2018, *MNRAS*, 481, 3148
Fadely, R., Willman, B., Geha, M., et al. 2011, *AJ*, 142, 88
Ferguson, P. S., & Strigari, L. E. 2019, *MNRAS*, submitted (arXiv:1909.11103)
Feroz, F., & Hobson, M. P. 2008, *MNRAS*, 384, 449
Feroz, F., Hobson, M. P., & Bridges, M. 2009, *MNRAS*, 398, 1601
Flaugher, B., Diehl, H. T., Honscheid, K., et al. 2015, *AJ*, 150, 150
Forbes, D. A., & Bridges, T. 2010, *MNRAS*, 404, 1203
Foreman-Mackey, D., Hogg, D. W., Lang, D., & Goodman, J. 2013, *PASP*, 125, 306
Frebel, A. 2018, *ARNPS*, 68, 237
Fritz, T. K., Battaglia, G., Pawłowski, M. S., et al. 2018, *A&A*, 619, A103
Fu, S. W., Simon, J. D., & Alarcón Jara, A. G. 2019, *ApJ*, 883, 11
Gaia Collaboration, Brown, A. G. A., Vallenari, A., et al. 2018, *A&A*, 616, A1
Garling, C., Willman, B., Sand, D. J., et al. 2018, *ApJ*, 852, 44
Garofalo, A., Cusano, F., Clementini, G., et al. 2013, *ApJ*, 767, 62
Geringer-Sameth, A., Koushiappas, S. M., & Walker, M. 2015, *ApJ*, 801, 74
Gilmore, G., Wilkinson, M. I., Wyse, R. F. G., et al. 2007, *ApJ*, 663, 948
Gnedin, O. Y., & Ostriker, J. P. 1997, *ApJ*, 474, 223
Górski, K. M., Hivon, E., Banday, A. J., et al. 2005, *ApJ*, 622, 759
Greco, C., Dall'Ora, M., Clementini, G., et al. 2008, *ApJL*, 675, L73
Harris, W. E. 1996, *AJ*, 112, 1487
Henden, A., & Munari, U. 2014, *CoSka*, 43, 518
Hernquist, L. 1990, *ApJ*, 356, 359
Homma, D., Chiba, M., Komiyama, Y., et al. 2019, *PASJ*, 71, 94
Homma, D., Chiba, M., Okamoto, S., et al. 2016, *ApJ*, 832, 21
Homma, D., Chiba, M., Okamoto, S., et al. 2018, *PASJ*, 70, S18
Hunter, J. D. 2007, *CSE*, 9, 90
Jahn, E. D., Sales, L. V., Wetzel, A., et al. 2019, *MNRAS*, 489, 5348
Jeon, M., Besla, G., & Bromm, V. 2017, *ApJ*, 848, 85
Jethwa, P., Erkal, D., & Belokurov, V. 2016, *MNRAS*, 461, 2212
Jethwa, P., Erkal, D., & Belokurov, V. 2018, *MNRAS*, 473, 2060

- Ji, A. P., Frebel, A., Chiti, A., & Simon, J. D. 2016, *Natur*, **531**, 610
- Ji, A. P., Simon, J. D., Frebel, A., Venn, K. A., & Hansen, T. T. 2019, *ApJ*, **870**, 83
- Johnson, J. A., Bolte, M., Stetson, P. B., Hesser, J. E., & Somerville, R. S. 1999, *ApJ*, **527**, 199
- Jones, E., Oliphant, T., Peterson, P., et al. 2001, SciPy: Open Source Scientific Tools for Python, <http://www.scipy.org/>
- Kallivayalil, N., Sales, L. V., Zivick, P., et al. 2018, *ApJ*, **867**, 19
- Kazantzidis, S., Lokas, E. L., Callegari, S., Mayer, L., & Moustakas, L. A. 2011, *ApJ*, **726**, 98
- Keller, S. C., Mackey, D., & Costa, G. S. D. 2011, *ApJ*, **744**, 57
- Kim, D., & Jerjen, H. 2015a, *ApJL*, **808**, L39
- Kim, D., & Jerjen, H. 2015b, *ApJ*, **799**, 73
- Kim, D., Jerjen, H., Mackey, D., Da Costa, G. S., & Milone, A. P. 2016, *ApJ*, **820**, 119
- Kim, S. Y., Peter, A. H. G., & Hargis, J. R. 2018, *PhRvL*, **121**, 211302
- Kirby, E. N., Boylan-Kolchin, M., Cohen, J. G., et al. 2013, *ApJ*, **770**, 16
- Kirby, E. N., Cohen, J. G., Simon, J. D., et al. 2017, *ApJ*, **838**, 83
- Kirby, E. N., Simon, J. D., & Cohen, J. G. 2015, *ApJ*, **810**, 56
- Koch, A., & Côté, P. 2019, *A&A*, **632**, A55
- Koposov, S., de Jong, J. T. A., Belokurov, V., et al. 2007, *ApJ*, **669**, 337
- Koposov, S. E., Belokurov, V., & Torrealba, G. 2017, *MNRAS*, **470**, 2702
- Koposov, S. E., Belokurov, V., Torrealba, G., & Evans, N. W. 2015, *ApJ*, **805**, 130
- Koposov, S. E., Walker, M. G., Belokurov, V., et al. 2018, *MNRAS*, **479**, 5343
- Kruijssen, J. M. D., Pfeffer, J. L., Reina-Campos, M., Crain, R. A., & Bastian, N. 2019, *MNRAS*, **486**, 3180
- Küpper, A. H. W., Johnston, K. V., Mieske, S., Collins, M. L. M., & Tollerud, E. J. 2017, *ApJ*, **834**, 112
- Laevens, B. P. M., Martin, N. F., Bernard, E. J., et al. 2015b, *ApJ*, **813**, 44
- Laevens, B. P. M., Martin, N. F., Ibata, R. A., et al. 2015a, *ApJL*, **802**, L18
- Laevens, B. P. M., Martin, N. F., Sesar, B., et al. 2014, *ApJL*, **786**, L3
- Leaman, R., VandenBerg, D. A., & Mendel, J. T. 2013, *MNRAS*, **436**, 122
- Li, T. S., Simon, J. D., Kuehn, K., et al. 2018, *ApJ*, **866**, 22
- Lokas, E. L., Kowalczyk, K., & Kazantzidis, S. 2012, *ApJ*, **751**, 61
- Lovell, M. R., Frenk, C. S., Eke, V. R., et al. 2014, *MNRAS*, **439**, 300
- Luque, E., Pieres, A., Santiago, B., et al. 2017, *MNRAS*, **468**, 97
- Luque, E., Queiroz, A., Santiago, B., et al. 2016, *MNRAS*, **458**, 603
- Luque, E., Santiago, B., Pieres, A., et al. 2018, *MNRAS*, **478**, 2006
- Macciò, A. V., & Fontanot, F. 2010, *MNRAS*, **404**, L16
- Mackey, A. D., & Gilmore, G. F. 2004, *MNRAS*, **355**, 504
- Mackey, A. D., Huxor, A. P., Ferguson, A. M. N., et al. 2010, *ApJL*, **717**, L11
- Marín-Franch, A., Aparicio, A., Piotto, G., et al. 2009, *ApJ*, **694**, 1498
- Marshall, J. L., Hansen, T., Simon, J. D., et al. 2019, *ApJ*, **882**, 177
- Martin, N. F., de Jong, J. T. A., & Rix, H.-W. 2008, *ApJ*, **684**, 1075
- Martin, N. F., Geha, M., Ibata, R. A., et al. 2016b, *MNRAS*, **458**, L59
- Martin, N. F., Ibata, R. A., Collins, M. L. M., et al. 2016a, *ApJ*, **818**, 40
- Martin, N. F., Nidever, D. L., Besla, G., et al. 2015, *ApJL*, **804**, L5
- Martínez-Vázquez, C. E., Vivas, A. K., Gurevich, M., et al. 2019, *MNRAS*, **490**, 2183
- Massari, D., Koppelman, H. H., & Helmi, A. 2019, *A&A*, **630**, L4
- Massari, D., Posti, L., Helmi, A., Fiorentino, G., & Tolstoy, E. 2017, *A&A*, **598**, L9
- Mau, S., Drlica-Wagner, A., Bechtol, K., et al. 2019, *ApJ*, **875**, 154
- McConnachie, A. W. 2012, *AJ*, **144**, 4
- Meylan, G., & Heggie, D. C. 1997, *A&ARv*, **8**, 1
- Morganson, E., Gruendl, R. A., Menanteau, F., et al. 2018, *PASP*, **130**, 074501
- Muñoz, R. R., Geha, M., Côté, P., et al. 2012, *ApJL*, **753**, L15
- Muñoz, R. R., Geha, M., & Willman, B. 2010, *AJ*, **140**, 138
- Mutlu-Pakdil, B., Sand, D. J., Walker, M. G., et al. 2019, arXiv:1907.07233
- Nadler, E. O., Gluscevic, V., Boddy, K. K., & Wechsler, R. H. 2019a, *ApJL*, **878**, L32
- Nadler, E. O., Mao, Y.-Y., Green, G. M., & Wechsler, R. H. 2019b, *ApJ*, **873**, 34
- Nadler, E. O., Mao, Y.-Y., Wechsler, R. H., Garrison-Kimmel, S., & Wetzel, A. 2018, *ApJ*, **859**, 129
- Nadler, E. O., Wechsler, R., Bechtol, K., et al. 2019c, *ApJ*, submitted (arXiv:1912.03303)
- Neilsen, E., Bernstein, G., Gruendl, R., & Kent, S. 2015, Limiting Magnitude, τ , T_{eff} , and Image Quality in DES Year 1, Technical Report FERMILAB-TM-2610-AE-CD
- Newton, O., Cautun, M., Jenkins, A., Frenk, C. S., & Helly, J. C. 2018, *MNRAS*, **479**, 2853
- Nidever, D. L., Majewski, S. R., & Butler Burton, W. 2008, *ApJ*, **679**, 432
- Nidever, D. L., Majewski, S. R., Butler Burton, W., & Nigra, L. 2010, *ApJ*, **723**, 1618
- Nidever, D. L., Olsen, K., Walker, A. R., et al. 2017, *AJ*, **154**, 199
- Pace, A. B., & Li, T. S. 2019, *ApJ*, **875**, 77
- Pardy, S. A., D'Onghia, E., Navarro, J., et al. 2020, *MNRAS*, **492**, 1543
- Pawlowski, M. S., & Kroupa, P. 2013, *MNRAS*, **435**, 2116
- Pawlowski, M. S., & Kroupa, P. 2020, *MNRAS*, **491**, 3042
- Pawlowski, M. S., Pflamm-Altenburg, J., & Kroupa, P. 2012, *MNRAS*, **423**, 1109
- Peñarrubia, J., Gómez, F. A., Besla, G., Erkal, D., & Ma, Y.-Z. 2016, *MNRAS*, **456**, L54
- Peñarrubia, J., Navarro, J. F., & McConnachie, A. W. 2008, *ApJ*, **673**, 226
- Piatek, S., & Pryor, C. 1995, *AJ*, **109**, 1071
- Plummer, H. C. 1911, *MNRAS*, **71**, 460
- Price-Whelan, A. M., Sipőcz, B. M., Günther, H. M., et al. 2018, *AJ*, **156**, 123
- Roderick, T. A., Jerjen, H., Mackey, A. D., & Da Costa, G. S. 2015, *ApJ*, **804**, 134
- Sales, L. V., Navarro, J. F., Kallivayalil, N., & Frenk, C. S. 2017, *MNRAS*, **465**, 1879
- Sand, D. J., Olszewski, E. W., Willman, B., et al. 2009, *ApJ*, **704**, 898
- Sand, D. J., Spekkens, K., Crnojević, D., et al. 2015, *ApJL*, **812**, L13
- Sand, D. J., Strader, J., Willman, B., et al. 2012, *ApJ*, **756**, 79
- Schlafly, E. F., & Finkbeiner, D. P. 2011, *ApJ*, **737**, 103
- Schlegel, D. J., Finkbeiner, D. P., & Davis, M. 1998, *ApJ*, **500**, 525
- Searle, L., & Zinn, R. 1978, *ApJ*, **225**, 357
- Simon, J. D. 2018, *ApJ*, **863**, 89
- Simon, J. D. 2019, *ARA&A*, **57**, 375
- Simon, J. D., Geha, M., Minor, Q. E., et al. 2011, *ApJ*, **733**, 46
- Simon, J. D., Li, T. S., Drlica-Wagner, A., et al. 2017, *ApJ*, **838**, 11
- Skrutskie, M. F., Cutri, R. M., Stiening, R., et al. 2006, *AJ*, **131**, 1163
- Smith, E. O., Rich, R. M., & Neill, J. D. 1998, *AJ*, **115**, 2369
- Torrealba, G., Belokurov, V., Koposov, S. E., et al. 2018, *MNRAS*, **475**, 5085
- Torrealba, G., Belokurov, V., Koposov, S. E., et al. 2019, *MNRAS*, **488**, 2743
- Van Der Walt, S., Colbert, S. C., & Varoquaux, G. 2011, *CSE*, **13**, 22
- Vivas, A. K., Olsen, K., Blum, R., et al. 2016, *AJ*, **151**, 118
- Walker, M. G., Mateo, M., Olszewski, E. W., et al. 2016, *ApJ*, **819**, 53
- Wetzel, A. R., Deason, A. J., & Garrison-Kimmel, S. 2015, *ApJ*, **807**, 49
- Wheeler, C., Hopkins, P. F., Pace, A. B., et al. 2019, *MNRAS*, **490**, 4447
- Willman, B., Blanton, M. R., West, A. A., et al. 2005a, *AJ*, **129**, 2692
- Willman, B., Dalcanton, J. J., Martínez-Delgado, D., et al. 2005b, *ApJL*, **626**, L85
- Willman, B., & Strader, J. 2012, *AJ*, **144**, 76
- Yozin, C., & Bekki, K. 2015, *MNRAS*, **453**, 2302
- Zinn, R. 1993, in ASP Conf. Ser. 48, The Globular Cluster-Galaxy Connection, ed. G. H. Smith & J. P. Brodie (San Francisco, CA: ASP), 38
- Zucker, D. B., Belokurov, V., Evans, N. W., et al. 2006a, *ApJL*, **650**, L41
- Zucker, D. B., Belokurov, V., Evans, N. W., et al. 2006b, *ApJL*, **643**, L103